3 Effective Electron-Electron Interaction in Many-Electron Systems

Ferdi Aryasetiawan
Mathematical Physics, Lund University,
Professorsgatan 1, 223 63 Lund, Sweden

Contents

E. Pavarini, E. Koch, A. Lichtenstein, and D. Vollhardt (eds.)
DMFT: From Infinite Dimensions to Real Materials
Modeling and Simulation Vol. 8
Forschungszentrum Jülich, 2018, ISBN 978-3-95806-313-6
http://www.cond-mat.de/events/correl18

1 Introduction

Were it not for the electron-electron (e-e) interaction in many-electron systems such as atoms, molecules and solids, we would not observe fascinating phenomena such as superconductivity, phase transitions, magnetism and many others. At the same time, it is this electron-electron interaction that makes solving the many-electron Hamiltonian exceedingly difficult. Solving the many-electron problem is perhaps one of the general goals in condensed matter theory. Direct methods for solving the many-electron Hamiltonian by, e.g., expanding the many-electron wave function as a linear combination of Slater determinants, are however not very fruitful when the number of electrons is large ($\sim 10^{23}$), which is the case in real materials. The number of Slater determinants required for a reasonably accurate solution becomes enormously large and unfeasible to handle in practice.

One successful approach for handling the many-electron problem is to first identify a subspace of the full Hilbert space in which e-e interaction plays a decisive role in determining the physical properties of interest. The basic idea is to treat the e-e interaction explicitly within the limited subspace whereas the influence of the rest of the Hilbert space is accounted for in a mean-field approximation. Thus the many-electron problem is reduced to a subspace and fortunately the size of the relevant subspace is in many cases relatively small compared to the full Hilbert space. However, the reduction of the many-electron problem to a limited subspace entails the need to renormalize the e-e interaction resulting in an effective interaction. Physically, the renormalization of the e-e interaction arises from the screening processes that have been eliminated when reducing the many-electron problem to the limited subspace.

A well-known example of an effective many-electron Hamiltonian is the Hubbard model [1], which in its simplest form is given by

$$H = -t \sum_{i \neq j,\sigma} c^{\dagger}_{i\sigma} c_{j\sigma} + U \sum_{i} n_{i\uparrow} n_{i\downarrow} \,. \tag{1}$$

The first term describes electron hopping with the same spin σ from site j to site i whereas the second term describes the interaction of electrons of opposite spin when they are on the same site i. The Hubbard model was introduced by Hubbard, Gutzwiller, and Kanamori at about the same time in the early 1960's as a phenomenological model to describe localized or semi-itinerant $3d$ states in transition metals. It is physically feasible that the bare e-e interaction is screened so that the on-site component of the screened interaction is the most important. The Hubbard model is well suited to study the electronic structure of strongly correlated systems in which on-site electron correlations are strong, due to the localized nature of the $3d$- or $4f$-orbitals. The model describes the competition between the kinetic energy represented by the hopping term and electron repulsion represented by the U term. For the half-filled case (one electron per site), as U becomes larger than t it is energetically more favorable for the electrons to be localized on their respective sites in order to avoid the large repulsion arising from having two electrons on the same site. As U increases further, each electron is locked on its site and the system turns into a Mott insulator. Since the Hubbard model is phenomenological, it is common practice to treat U/t as a parameter.

In the simplest form there is only one orbital per site but in general there can be several orbitals per site so that the hopping parameter t and the effective e-e interaction U (the Hubbard U) are matrices instead of single numbers

$$H = \sum_{\mathbf{R}i,\mathbf{R}'j,\sigma} t^{\sigma}_{\mathbf{R}i,\mathbf{R}'j}\, c^{\dagger}_{\mathbf{R}i\sigma} c_{\mathbf{R}'j\sigma} + \frac{1}{2} \sum_{\mathbf{R},\mathbf{R}',ijkl,\sigma\sigma'} U^{\sigma\sigma'}_{ijkl}(\mathbf{R},\mathbf{R}')\, c^{\dagger}_{\mathbf{R}i\sigma} c^{\dagger}_{\mathbf{R}'j\sigma'} c_{\mathbf{R}'k\sigma'} c_{\mathbf{R}l\sigma}\,. \tag{2}$$

A set of localized orbitals $\{\varphi_{\mathbf{R}i\sigma}\}$ defining the annihilation and creation operators are assumed. The subscripts $\mathbf{R}$ and i label the site and the orbital, while σ denotes the spin variable. The parameters $U^{\sigma\sigma'}_{ijkl}(\mathbf{R},\mathbf{R}')$ are the matrix elements of the effective e-e interaction $U(\mathbf{r},\mathbf{r}')$

$$U^{\sigma\sigma'}_{ijkl}(\mathbf{R},\mathbf{R}') = \int d^3r d^3r'\, \varphi^{*}_{\mathbf{R}i}(\mathbf{r}) \varphi^{*}_{\mathbf{R}'j}(\mathbf{r}')\, U(\mathbf{r},\mathbf{r}')\, \varphi_{\mathbf{R}'k}(\mathbf{r}') \varphi_{\mathbf{R}l}(\mathbf{r}). \tag{3}$$

We have assumed that the effective interaction is static and orbitals with the same position variable belong to the same atomic site. In general U depends on four atomic sites.

In the last couple of decades there has been an increasing interest in combining the Hubbard model with realistic band structure calculations in order to study the electronic structure of strongly correlated materials from which various physical properties can be derived. Each material is then characterized by hopping parameters $t^{\sigma}_{\mathbf{R}i,\mathbf{R}'j}$, which determine the underlying one-particle band structure, and by $U^{\sigma\sigma'}_{ijkl}(\mathbf{R},\mathbf{R}')$, which determine the effective e-e interaction. The hopping parameters can be determined from realistic band structure calculations, commonly done within the local density approximation (LDA) [2], by a tight-binding fit. However, it is much less obvious how to determine the effective e-e interaction. If we wish to make quantitative predictions about the physical properties of a material, it is necessary to compute the matrix U from first-principles, rather than treating it as an adjustable parameter. A model Hamiltonian with adjustable parameters runs the risk of producing certain properties in good agreement with experiment not for a theoretically justifiable reason but rather due to a fortuitous cancellation between an inappropriate choice of the parameters and inaccurate theoretical approximations employed in solving the model.

The purpose of this lecture is to describe a systematic way of determining the effective e-e interaction corresponding to a chosen subspace into which the many-electron problem is downfolded. The method is quite general and it yields $U(\mathbf{r},\mathbf{r}';\omega)$ so not only local but also non-local matrix elements can be extracted. Moreover, the method delivers a frequency-dependent U, which encapsulates the dynamics of the screening processes determining the effective e-e interaction in the chosen subspace. The resulting effective interaction can be used in a model Hamiltonian or in an effective-action formalism, which is then solved by using many-body techniques such as dynamical mean-field theory (DMFT) [3] and quantum Monte Carlo methods.

2 Theory

The determination of the Hubbard U has a long history. Perhaps the earliest attempt was made by Herring [4] who defined U as the energy cost of transferring an electron between two atoms

in a crystal. If $E(N)$ is the energy per atom in the initial configuration with N electrons, removing an electron from a given site costs $E(N-1) - E(N)$ and putting the removed electron to another site costs $E(N+1) - E(N)$ so the total cost is then

$$\begin{aligned} U &= \big[E(N+1) - E(N)\big] + \big[E(N-1) - E(N)\big] \\ &= E(N+1) - 2E(N) + E(N-1). \end{aligned} \tag{4}$$

We are usually interested in U associated with localized orbitals such as the $3d$-orbitals of transition metals or the $4f$-orbitals of the lanthanides. If n_d labels the occupation number of a $3d$-orbital, treating it as a continuous variable we may write Eq. (4) as

$$U = \frac{\partial^2 E}{\partial n_d^2}\,. \tag{5}$$

The change in the total energy associated with the change in the occupation number is given by $\delta E = \varepsilon_d \delta n_d$, where ε_d is the orbital energy, so that U can be expressed as the change in the orbital energy with respect to the occupation number:

$$U = \frac{\partial}{\partial n_d}\left(\frac{\partial E}{\partial n_d}\right) = \frac{\partial \varepsilon_d}{\partial n_d}\,. \tag{6}$$

Early calculations of U for transition metals using this formula were made by Cox *et al.* [5]. The eigenvalues are calculated for the three different configurations $3d^n4s^1$, $3d^{n+1}4s^0$, $3d^{n-1}4s^2$ by solving an atomic problem self-consistently with an appropriate boundary condition at the Wigner-Seitz sphere boundary to mimic the atomic environment in the crystal. The change in the atomic wave function from configuration $3d^n4s^1$ to configurations $3d^{n+1}4s^0$ and $3d^{n-1}4s^2$ captures, respectively, the effects of screening arising from adding and removing an electron from the $3d$-shell. The result shows an almost linear increase across the $3d$-series from 1.3 eV for Sc to 3.3 eV for Ni. A similar approach was also employed by Herbst [6] to compute U for the $4f$-series.

A constrained LDA (cLDA) approach was later introduced by Dederichs *et al.* [7] who used it to compute U for Ce. The total energy as a function of the $4f$ occupation number is given by

$$E(n_f) = \min\left\{E[\rho(\mathbf{r})] + v_f\left(\int_{R_S} d^3r\rho_f(\mathbf{r}) - n_f\right)\right\}, \tag{7}$$

where R_S is the radius of the Wigner-Seitz sphere, n_f and ρ_f are respectively the occupation number and density of the $4f$-orbital and v_f is a Lagrange multiplier corresponding to the constraint that the occupation number of the $4f$-orbital is given by n_f. The Lagrange multiplier v_f can be interpreted as a constant projection potential that acts only on the $4f$-orbitals. The constraint only applies to the $4f$-electrons while other electrons (spd) within the atomic sphere as well as in the neighboring cells can relax in the self-consistency cycle to minimize the total energy. By calculating $E(n_f)$ in Eq. (7) as a function of n_f around the unconstrained equilibrium value the Hubbard U can then be computed using the formula in Eq. (5).

The cLDA method can also be formulated using the supercell approach in which the constraint is implemented by cutting off hopping integrals from the $3d/4f$-orbitals in the central atom in

the supercell to neighboring atoms, thus fixing the number of the $3d/4f$-electrons, while other electrons can relax and screen the $3d/4f$-electrons [8]. Hybertsen *et al.* [9] and Cococcioni and Gironcoli [10] improved the cLDA method by taking into account the change in the kinetic energy, the latter based on linear response theory.
In this note, we will describe a different method based on the idea that the effective e-e interaction in the chosen subspace corresponding to the model Hamiltonian must be such that when it is screened by the electrons in the model, it reproduces the fully screened interaction of the real system. This suggests that screening channels associated with the model must be removed when computing U [11].

2.1 Screening and screened potential

The underlying concept common to methods for determining U is screening. Consider a many-electron system such as a solid in its ground state and let us apply a time-dependent external field $V_{\rm ext}(\mathbf{r},t)$. We wish to study within linear response theory how this external potential is screened by the electrons in the system. The external field induces a change in the electron density, which is given by

$$\rho_{\rm ind}(\mathbf{r},t) = \int d^3r' dt'\, R(\mathbf{r},\mathbf{r}';t-t')\, V_{\rm ext}(\mathbf{r}',t')\,, \tag{8}$$

where $R(\mathbf{r},\mathbf{r}';t-t')$ is the linear density response function, which depends only on the relative time $t-t'$ since the Hamiltonian of the system is assumed to be time-independent, and it is a property of the system, independent of the applied external field $V_{\rm ext}$. The induced density $\rho_{\rm ind}$, in turn, generates an induced potential

$$V_{\rm ind}(\mathbf{r},t) = \int d^3r'\, v(\mathbf{r}-\mathbf{r}')\, \rho_{\rm ind}(\mathbf{r}',t)\,, \tag{9}$$

where $v(\mathbf{r}-\mathbf{r}') = 1/|\mathbf{r}-\mathbf{r}'|$ is the Coulomb interaction. The total potential or the screened potential is then given by

$$V_{\rm scr}(\mathbf{r},t) = V_{\rm ext}(\mathbf{r},t) + V_{\rm ind}(\mathbf{r},t)\,. \tag{10}$$

Using $V_{\rm ind}$ in Eq. (9) and $\rho_{\rm ind}$ in Eq. (8) we find

$$\begin{aligned} V_{\rm scr}(\mathbf{r},t) &= V_{\rm ext}(\mathbf{r},t) + \int d^3r'\, v(\mathbf{r}-\mathbf{r}')\, \rho_{\rm ind}(\mathbf{r}',t) \\ &= V_{\rm ext}(\mathbf{r},t) + \int d^3r'\, v(\mathbf{r}-\mathbf{r}') \int d^3r''\, dt' R(\mathbf{r}',\mathbf{r}'';t-t')\, V_{\rm ext}(\mathbf{r}'',t')\,. \end{aligned} \tag{11}$$

It is convenient to work in frequency space by using the Fourier transform defined according to

$$f(\omega) = \int dt\, e^{i\omega t} f(t) \qquad \text{and} \quad f(t) = \int \frac{d\omega}{2\pi} e^{-i\omega t} f(\omega)\,. \tag{12}$$

Since the second term in the last line of Eq. (11) is a convolution in time, applying the Fourier transform to Eq. (11) yields

$$V_{\rm scr}(\mathbf{r},\omega) = V_{\rm ext}(\mathbf{r},\omega) + \int d^3r' d^3r''\, v(\mathbf{r}-\mathbf{r}')\, R(\mathbf{r}',\mathbf{r}'';\omega)\, V_{\rm ext}(\mathbf{r}'',\omega)\,, \tag{13}$$

Regarding Eq. (13) as a matrix equation we have

$$V_{\rm scr}(\omega) = \big[1 + vR(\omega)\big] V_{\rm ext}(\omega)\,, \tag{14}$$

which allows us to identify $1 + vR(\omega)$ as the inverse dielectric matrix

$$\epsilon^{-1}(\omega) = 1 + vR(\omega). \tag{15}$$

2.2 Screened Coulomb interaction

We can now apply the general formulation in the previous section to write down the screened Coulomb interaction. As the external field we consider the instantaneous bare electron-electron interaction

$$V_{\rm ext}(\mathbf{r}t, \mathbf{r}'t') = v(\mathbf{r} - \mathbf{r}')\,\delta(t - t')\,, \tag{16}$$

where we treat $(\mathbf{r}', t')$ as parameters. Without loss of generality we may set $t' = 0$. This external field can be interpreted as an instantaneous Coulomb potential at point $\mathbf{r}$ arising from a point charge located at $\mathbf{r}'$. Its Fourier transform is given by

$$V_{\rm ext}(\mathbf{r}, \mathbf{r}'; \omega) = v(\mathbf{r} - \mathbf{r}')\,. \tag{17}$$

Since

$$\delta(t - t') = \int \frac{d\omega}{2\pi} e^{-i\omega(t-t')}\,, \tag{18}$$

the external field $v(\mathbf{r}-\mathbf{r}')\,\delta(t-t')$ can also be regarded as a superposition of harmonic potentials with a common strength $v(\mathbf{r} - \mathbf{r}')$. From Eq. (13) the screened Coulomb interaction, which we now call W, fulfills the equation

$$\begin{aligned} W(\mathbf{r}, \mathbf{r}'; \omega) &= v(\mathbf{r} - \mathbf{r}') + \int d^3r_1 d^3r_2\, v(\mathbf{r} - \mathbf{r}_1)\, R(\mathbf{r}_1, \mathbf{r}_2; \omega)\, v(\mathbf{r}_2 - \mathbf{r}') \\ &= \int d^3r''\, \epsilon^{-1}(\mathbf{r}, \mathbf{r}''; \omega)\, v(\mathbf{r}'' - \mathbf{r}')\,, \end{aligned} \tag{19}$$

where we have used the definition of the inverse dielectric matrix in Eq. (15). In other words, $W(\mathbf{r}, \mathbf{r}'; \omega) \exp(-i\omega t)$ is the screened interaction of the external field $v(\mathbf{r} - \mathbf{r}') \exp(-i\omega t)$. The screened Coulomb interaction W plays an important role in Green function theory since it determines the self-energy, e.g., in the Hedin equations [12–14].
We may introduce a polarization function defined as

$$\rho_{\rm ind}(\mathbf{r}, t) = \int d^3r' dt'\, P(\mathbf{r}, \mathbf{r}'; t - t')\, V_{\rm scr}(\mathbf{r}', t')\,, \tag{20}$$

i.e., as a response function but defined with respect to the screened potential given in Eq. (10). We therefore have from Eq. (8)

$$\rho_{\rm ind} = RV_{\rm ext} = PV_{\rm scr} = P\,(V_{\rm ext} + V_{\rm ind}). \tag{21}$$

Since

$$V_{\rm ind} = v\rho_{\rm ind} = vRV_{\rm ext} \tag{22}$$

we obtain

$$RV_{\rm ext} = P\left(1 + vR\right)V_{\rm ext}\,. \tag{23}$$

Since $V_{\rm ext}$ is arbitrary, we find

$$R = P\left(1 + vR\right) = P\epsilon^{-1}. \tag{24}$$

In terms of the polarization function the screened interaction in Eq. (19) can then be written as

$$W = v + vRv = v + vP\epsilon^{-1}v = v + vPW. \tag{25}$$

Solving for W we find

$$W = [1 - vP]^{-1}v, \tag{26}$$

which allows us to identify the dielectric matrix as

$$\epsilon = 1 - vP. \tag{27}$$

2.3 Linear density response function

The exact expression for the linear density response function (hereafter referred to as response function) was derived by Kubo using time-dependent perturbation theory [15]. It can also be derived more conveniently using Green function theory in the interaction representation described in the Appendix. The exact expression for the time-ordered response function is given by

$$iR(1,2) = \langle\Psi_0|\Delta\hat{\rho}_H(2)\Delta\hat{\rho}_H(1)|\Psi_0\rangle\ \theta(t_2 - t_1) + \langle\Psi_0|\Delta\hat{\rho}_H(1)\Delta\hat{\rho}_H(2)|\Psi_0\rangle\ \theta(t_1 - t_2)\,, \tag{28}$$

where we have used the notation $1 = (\mathbf{r}_1, t_1)$, etc., Ψ_0 is the many-electron ground state and

$$\Delta\hat{\rho}_H(1) = \hat{\rho}_H(1) - \rho(1) \tag{29}$$

is the density fluctuation operator in the Heisenberg picture

$$\Delta\hat{\rho}_H(\mathbf{r}, t) = e^{i\hat{H}t}\Delta\hat{\rho}(\mathbf{r})e^{-i\hat{H}t}. \tag{30}$$

$\hat{H}$ is the Hamiltonian of the many-electron system, assumed to be independent of time.
The Fourier transform of the response function is given by (see Appendix)

$$R(\mathbf{r}, \mathbf{r}'; \omega) = \sum_n \left[\frac{\langle\Psi_0|\Delta\hat{\rho}(\mathbf{r})\,|\Psi_n\rangle\,\langle\Psi_n|\,\Delta\hat{\rho}(\mathbf{r}')|\Psi_0\rangle}{\omega - E_n + E_0 + i\eta} - \frac{\langle\Psi_0|\Delta\hat{\rho}(\mathbf{r}')\,|\Psi_n\rangle\,\langle\Psi_n|\,\Delta\hat{\rho}(\mathbf{r})|\Psi_0\rangle}{\omega + E_n - E_0 - i\eta}\right], \tag{31}$$

where $\hat{H}|\Psi_n\rangle = E_n|\Psi_n\rangle$. The term $n = 0$, corresponding to the ground state, is zero since $\langle\Psi_0|\Delta\hat{\rho}(\mathbf{r})|\Psi_0\rangle = 0$.

2.4 Random phase approximation

For real materials it is virtually impossible to compute the exact response function, so in practice we must resort to approximations. The most successful approximation is the random phase approximation (RPA) developed by Bohm and Pines in the 1950's [16]. The RPA was originally derived from the equation of motion for the density fluctuation. Some years later Gell-Mann and Brueckner derived the RPA using a diagrammatic technique. It was later recognized that the RPA can be regarded simply as the time-dependent Hartree approximation, which can be seen most clearly within Green function theory described in the Appendix.
In the RPA, it is assumed that the density response of the many-electron system to an external perturbation is the same as the response to the screened potential, $V_{\rm scr} = V_{\rm ext} + V_{\rm ind}$, but as if the system is non-interacting. Thus, if P^0 is the non-interacting response function corresponding to some mean-field approximation for the many-electron system, then schematically

$$\rho_{\rm ind} = RV_{\rm ext} = P^0(V_{\rm ext} + V_{\rm ind}). \tag{32}$$

Since $V_{\rm ind} = v\rho_{\rm ind} = vRV_{\rm ext}$ and $V_{\rm ext}$ is arbitrary, we obtain

$$R = P^0 + P^0 vR\,. \tag{33}$$

It is the same equation as Eq. (24) except that P has been replaced by P^0. The time-ordered non-interacting response function is given by (see Appendix)

$$P^0(\mathbf{r},\mathbf{r}';\omega) = -2\sum_i^{\rm occ}\sum_j^{\rm unocc}\left(\frac{f_{ij}(\mathbf{r},\mathbf{r}')}{\omega+(\varepsilon_j-\varepsilon_i-i\delta)} - \frac{f^*_{ij}(\mathbf{r},\mathbf{r}')}{\omega-(\varepsilon_j-\varepsilon_i-i\delta)}\right), \tag{34}$$

where

$$f_{ij}(\mathbf{r},\mathbf{r}') = \psi_i(\mathbf{r})\psi^*_j(\mathbf{r})\psi^*_i(\mathbf{r}')\psi_j(\mathbf{r}'). \tag{35}$$

It can also be obtained from the exact expression for the response function in Eq. (31) by using non-interacting many-electron states (single Slater determinants). The factor of two accounts for the two spin channels in the paramagnetic case and for a spin-polarized system we add up the polarization from each channel. $\{\psi_i,\varepsilon_i\}$ are the eigenfunctions and eigenvalues of the non-interacting system, which are commonly chosen to be those of the LDA.
In practice both the polarization function and the response function are expanded according to

$$P(\mathbf{r},\mathbf{r}';\omega) = \sum_{\mathbf{k}\alpha\beta} B_{\mathbf{k}\alpha}(\mathbf{r})P_{\alpha\beta}(\mathbf{k},\omega)B^*_{\mathbf{k}\beta}(\mathbf{r}'), \tag{36}$$

where $\{B_{\mathbf{k}\alpha}\}$ is a set of (two-particle) basis functions fulfilling the Bloch theorem

$$B_{\mathbf{k}\alpha}(\mathbf{r}+\mathbf{T}) = e^{i\mathbf{k}\cdot\mathbf{T}}B_{\mathbf{k}\alpha}(\mathbf{r}). \tag{37}$$

For example, $B_{\mathbf{k}\alpha}(\mathbf{r}) = \exp[i(\mathbf{k}+\mathbf{G})\cdot\mathbf{r}]$, in which the label α denotes the reciprocal lattice vector $\mathbf{G}$. Another example is a product basis [14] based on the linear muffin-tin orbital (LMTO)

method [17]:

$$B_{\mathbf{k}\alpha}(\mathbf{r}) = \sum_{\mathbf{T}} e^{i\mathbf{k}\cdot\mathbf{T}} b_{\mathbf{R}\alpha}(\mathbf{r}-\mathbf{T}), \tag{38}$$

$$b_{\mathbf{R}\alpha}(\mathbf{r}) = \chi_{\mathbf{R}L}(\mathbf{r})\chi_{\mathbf{R}L'}(\mathbf{r}), \tag{39}$$

where $\chi_{\mathbf{R}L}$ is an LMTO centered at atom $\mathbf{R}$ with angular momentum L and $\alpha = (L, L')$. It is worth noting that the basis $\{B_{\mathbf{k}\alpha}\}$ is by construction complete for P and R, but it is not in general complete for W. As can be seen in Eq. (19), to expand W a complete basis for the bare Coulomb interaction is needed.

2.5 The constrained RPA method

Our aim is to determine the effective e-e interaction among electrons residing in a given subspace, which can represent a partially filled narrow band across the Fermi level typically originating from $3d$- or $4f$-orbitals found in strongly correlated systems. The physical assumption is that when the effective e-e interaction is screened by electrons residing in the subspace, the resulting screened interaction should reproduce the screened interaction of the full system [11]. If P is the polarization of the full many-electron system the screened interaction is given by

$$W = v + vPW. \tag{40}$$

Let P^d be the polarization of the subspace such as the $3d$- or $4f$-band in the Hubbard model. We refer to this subspace as d-subspace and the rest of the Hilbert space as r-subspace. We require that

$$W = U + UP^dW \tag{41}$$

$$= \left(1 - UP^d\right)^{-1} U \tag{42}$$

which defines U as the effective e-e interaction in the d subspace. It is given by

$$U = W\left(1 - P^dW\right)^{-1}. \tag{43}$$

Within the RPA, $P = P^0$ as given in Eq. (34) and P^d is given by the same expression except that the single-particle wave functions are restricted to those of the d-subspace. Eq. (43) provides an operational means for computing U.

Alternatively, U can be written in a physically more transparent form. The total polarization can be decomposed according to

$$P = P^d + P^r, \tag{44}$$

which is illustrated in Fig. 1. From Eq. (26) we have [11]

$$\begin{aligned} W &= (1 - vP)^{-1} v \\ &= (1 - vP^r - vP^d)^{-1} v \\ &= \left((1 - vP^r)\left(1 - (1 - vP^r)^{-1} vP^d\right)\right)^{-1} v \\ &= \left(1 - (1 - vP^r)^{-1} vP^d\right)^{-1} (1 - vP^r)^{-1} v \end{aligned}$$

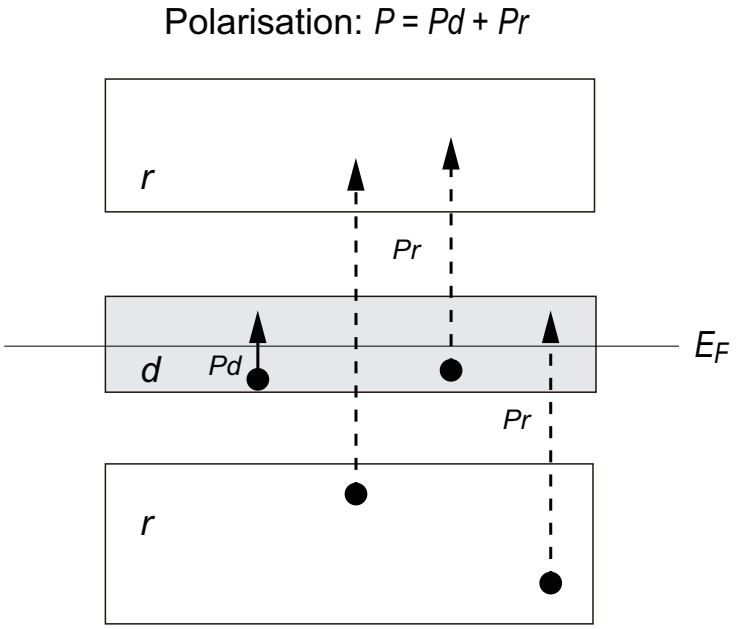

Fig. 1: *Schematic illustration of the definitions of P^d and P^r. The former is confined to transitions inside the d-subspace whereas the latter contains both transitions inside the r-subspace as well as between the d- and r-subspaces.*

Upon comparison with Eq. (42) we can verify that U

$$U = (1 - vP^r)^{-1}v \tag{45}$$

$$U = v + vP^rU \tag{46}$$

which is consistent with the interpretation of U as the effective e-e interaction in the d-subspace since the bare interaction v is screened by P^r, which consists of those polarization channels that do not include the channels within the d-subspace.
Similar to the screened interaction W in Eq. (19) we may write

$$U = v + vR^rv, \tag{47}$$

where R^r satisfies

$$R^r = P^r + P^rvR^r, \tag{48}$$

$$R^r = (1 - P^rv)^{-1}P^r. \tag{49}$$

Writing out in full in position representation we obtain

$$U(\mathbf{r}, \mathbf{r}'; \omega) = v(\mathbf{r} - \mathbf{r}') + \int d^3r_1 d^3r_2\, v(\mathbf{r} - \mathbf{r}_1)\, R^r(\mathbf{r}_1, \mathbf{r}_2; \omega)\, v(\mathbf{r}_2 - \mathbf{r}')\,. \tag{50}$$

Expanding R^r as in Eq. (36) we obtain

$$U(\mathbf{r}, \mathbf{r}'; \omega) = v(\mathbf{r} - \mathbf{r}') + \sum_{\mathbf{k}\alpha\beta} C_{\mathbf{k}\alpha}(\mathbf{r}) R^r_{\alpha\beta}(\mathbf{k}, \omega) C^*_{\mathbf{k}\beta}(\mathbf{r}'), \tag{51}$$

where

$$C_{\mathbf{k}\alpha}(\mathbf{r}) = \int d^3r_1\, v(\mathbf{r}-\mathbf{r}_1)\, B_{\mathbf{k}\alpha}(\mathbf{r}_1)\,. \tag{52}$$

The constrained RPA (cRPA) method provides an effective e-e interaction as a function of positions $(\mathbf{r},\mathbf{r}')$ and frequency ω from which matrix elements of U, both local and non-local, needed as input in a model Hamiltonian can be extracted. Since the d-subspace usually corresponds to a partially filled narrow band across the Fermi level, as illustrated in Fig. 1, P^d contains the metallic screening whereas $P^r = P - P^d$, which determines U, contains no metallic screening so that U is intrinsically long range since the screening is incomplete, similar to the screened interaction in semiconductors and insulators.

2.6 Wannier orbitals

In most applications involving strongly correlated systems, we need to define a set of localized orbitals defining the annihilation and creation operators in the model Hamiltonian.The choice of localized orbitals is arbitrary. For example, they could be a set of pre-processed linearized muffin-tin orbitals (LMTO) [17] or a set of post-processed maximally localized Wannier orbitals [18] constructed from Bloch eigenstates generated from a band structure calculation. The Wannier function with band index n at cell $\mathbf{R}$ is defined by

$$|\varphi_{\mathbf{R}n}\rangle = \frac{\Omega}{(2\pi)^3}\int_{BZ} d^3k\, e^{-i\mathbf{k}\cdot\mathbf{R}}|\psi^{(\mathrm{w})}_{\mathbf{k}n}\rangle, \tag{53}$$

where Ω is the cell volume and $|\psi^{(\mathrm{w})}_{n\mathbf{k}}\rangle$ is a linear combination of the eigenfunctions of a mean-field Hamiltonian

$$|\psi^{(\mathrm{w})}_{\mathbf{k}n}\rangle = \sum_m |\psi_{\mathbf{k}m}\rangle\, \mathcal{U}_{mn}(\mathbf{k}). \tag{54}$$

In practical implementations, the Kohn-Sham wavefunctions are usually used for $|\psi_{\mathbf{k}m}\rangle$. In the maximally localized Wannier function scheme, the coefficients $\mathcal{U}_{mn}(\mathbf{k})$'s are determined by minimizing the extent of the Wannier orbitals [18]

$$\Omega = \sum_n (\langle\varphi_{\mathbf{0}n}|r^2|\varphi_{\mathbf{0}n}\rangle - |\langle\varphi_{\mathbf{0}n}|\mathbf{r}|\varphi_{\mathbf{0}n}\rangle|^2). \tag{55}$$

After defining a set of localized orbitals we now compute the matrix elements of U in these orbitals. From Eq. (51), taking the matrix elements of U as defined in Eq. (3), we obtain

$$U^{\sigma\sigma'}_{ijkl}(\mathbf{R},\mathbf{R}';\omega) = v^{\sigma\sigma'}_{ijkl}(\mathbf{R},\mathbf{R}') + \sum_{\mathbf{k}\alpha\beta}\langle\varphi_{\mathbf{R}i}\varphi^*_{\mathbf{R}l}|C_{\mathbf{k}\alpha}\rangle R^r_{\alpha\beta}(\mathbf{k},\omega)\langle C_{\mathbf{k}\beta}|\varphi^*_{\mathbf{R}'j}\varphi_{\mathbf{R}'k}\rangle, \tag{56}$$

where $C_{\mathbf{k}\alpha}$ is defined in Eq. (52) and

$$U^{\sigma\sigma'}_{ijkl}(\mathbf{R},\mathbf{R}';\omega) = \int d^3r d^3r' \varphi^*_{\mathbf{R}i}(\mathbf{r})\varphi^*_{\mathbf{R}'j}(\mathbf{r}')U(\mathbf{r},\mathbf{r}';\omega)\varphi_{\mathbf{R}'k}(\mathbf{r}')\varphi_{\mathbf{R}l}(\mathbf{r}). \tag{57}$$

2.7 cRPA for entangled bands

For isolated bands the Wannier orbitals are well defined and they reproduce the bands. However, in many applications it may happen that the narrow bands which are to be modelled are not isolated so the Wannier orbitals are not unique. For this case, we optimize $\mathcal{U}_{mn}(\mathbf{k})$ with m limited to the states inside a chosen energy window. For a given $\mathbf{k}$-point the number of bands is equal to or larger than the number of m. The Wannier functions are more localized the larger the energy window, since optimization is done in a wider Hilbert space. The band structure $\{\tilde{\psi}_{\mathbf{k}m}, \tilde{\varepsilon}_{\mathbf{k}m}\}$ computed using these Wannier orbitals will not in general reproduce the original band structure. $\{\tilde{\psi}_{\mathbf{k}m}\}$ define the d-subspace and we introduce the projection operator [19]

$$P_{\mathbf{k}} = \sum_m |\tilde{\psi}_{\mathbf{k}m}\rangle\langle\tilde{\psi}_{\mathbf{k}m}|. \tag{58}$$

We define the r-subspace as follows:

$$|\phi_{\mathbf{k}n}\rangle = (1 - P_{\mathbf{k}})|\psi_{\mathbf{k}n}\rangle, \tag{59}$$

where $\{\psi_{\mathbf{k}n}\}$ are the original Bloch states. The states $\{\phi_{\mathbf{k}n}\}$ are not orthonormal but they are evidently orthogonal to the d-subspace. The one-particle Hamiltonian is now calculated using $\{\tilde{\psi}_{\mathbf{k}m}\}$ and $\{\phi_{\mathbf{k}n}\}$ as basis functions, but as an approximation, the coupling between the d- and r-subspaces is set to zero

$$H = \begin{bmatrix} H_{dd} & 0 \\ 0 & H_{rr} \end{bmatrix}, \tag{60}$$

where H_{dd} is the Hamiltonian matrix calculated in the d-subspace, which is already diagonal, $\{\tilde{\psi}_{\mathbf{k}m}\}$ and H_{rr} is calculated in the subspace of $\{\phi_{\mathbf{k}n}\}$.
The total polarization function is then computed from the new disentangled band structure obtained from the Hamiltonian in Eq. (60) and P^d is computed from $\{\tilde{\psi}_{\mathbf{k}m}, \tilde{\varepsilon}_{\mathbf{k}m}\}$. It would seem reasonable to use the total polarization function P calculated from the original band structure but this procedure leads to oscillations in U at low energy due to the presence of low-lying polarizations not completely eliminated from P when calculating $P^r = P - P^d$.

3 Examples

In the following we will describe applications of the cRPA method to some real materials to illustrate what information can be extracted from the calculations.

3.1 Cubic perovskite $SrVO_3$

As a first example, we consider a prototype of a correlated metal, the cubic perovskite $SrVO_3$. This example has been considered before in Ref. [20] but it is included here since it provides an ideal illustration for the cRPA method. As can be seen in Fig. 2 the t_{2g}-bands cross the Fermi level and are well isolated from other bands. These three t_{2g}-bands form the d-subspace, which

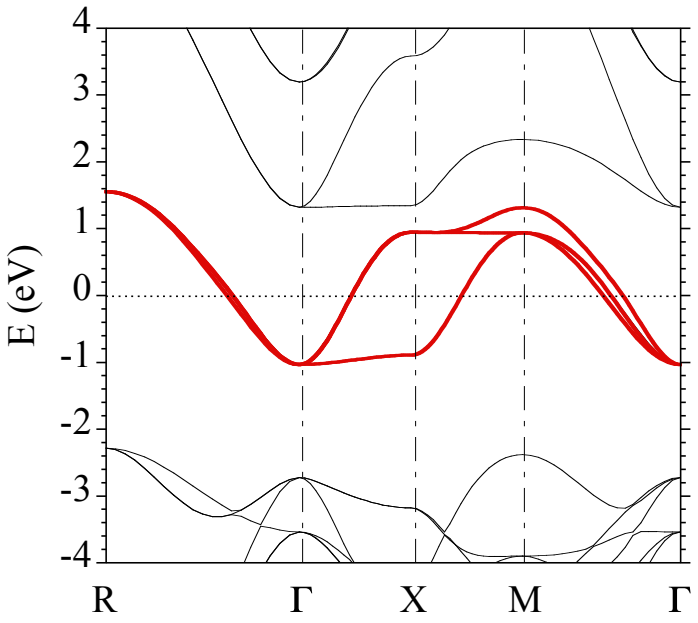

Fig. 2: *The LDA band structure of metallic $SrVO_3$ with cubic perovskite structure. The red lines correspond to the three t_{2g}-bands which define the d-subspace and are isolated from the rest of the bands [20].*

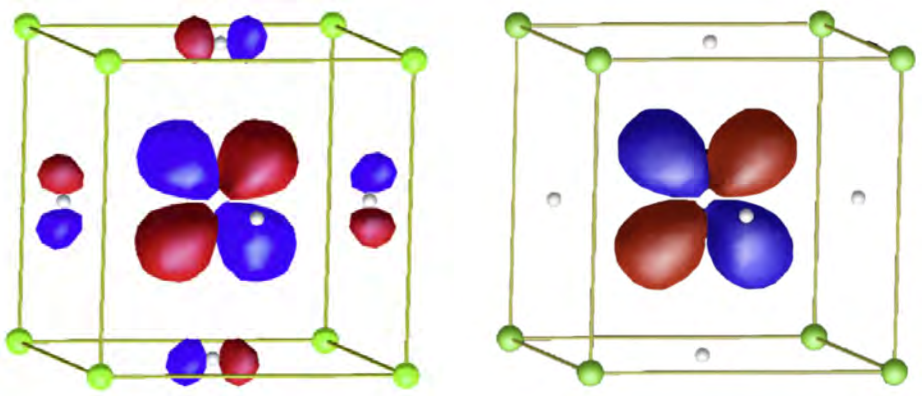

Fig. 3: *The maximally localized Wannier functions of $SrVO_3$ centered at vanadium of xy, yz, or xz character. If the horizontal and vertical directions are respectively assigned to be the x and z axes the shown Wannier function corresponds to xz character. The red (blue) represents the positive (negative) contour. (Green sphere = strontium, white sphere = oxygen). Left figure: The Wannier orbital is constructed from the vanadium t_{2g}-bands only. We note that the Wannier function has tails on the oxygen sites. Right figure: The Wannier orbital is constructed from the vanadium $(t_{2g} + e_g)$- bands and oxygen p-bands, which makes it clearly more localized on the vanadium site compared to the one on the left figure [20].*

corresponds to the Hilbert space of the Hubbard model. One of the Wannier orbitals constructed from these t_{2g}-bands is shown on Fig. 3 (left). If the d-subspace is extended to include the e_g-bands and the oxygen p-bands, the Wannier orbitals of t_{2g}-symmetry become more localized, as can be seen on the right figure of Fig. 3.

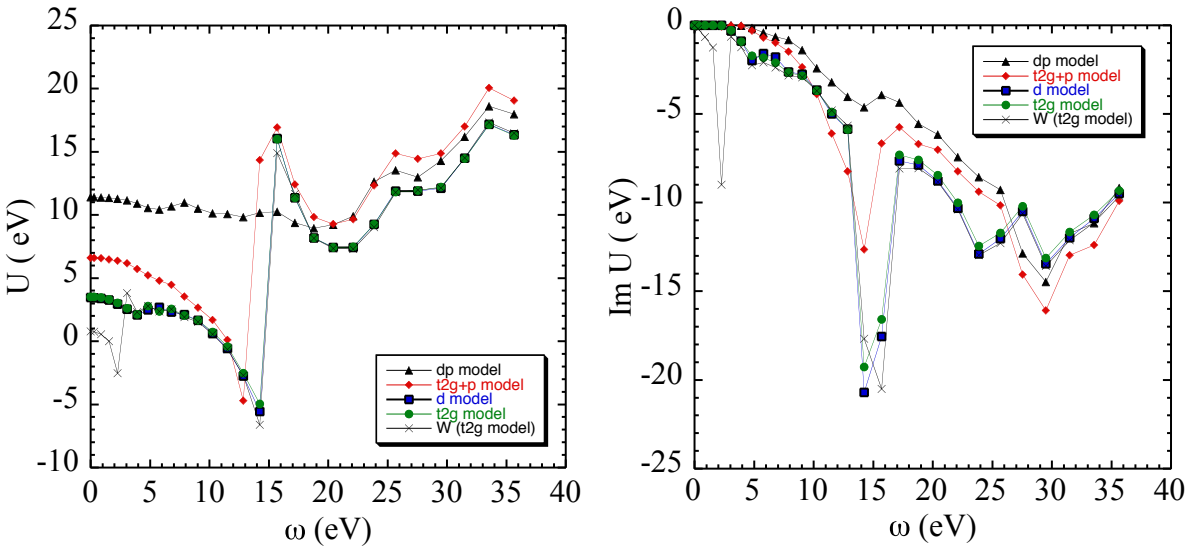

Fig. 4: *Illustration of how the on-site Hubbard* $U = U^{\sigma\sigma}_{iiii}(\mathbf{R}, \mathbf{R}; \omega)$ *depends on the choice of the* d*-subspace indicated by the legends in the figure. The subscript* i *labels one of the* t_{2g}*-orbitals* (xy, yz, *or* xz) *and* $\mathbf{R}$ *labels the vanadium atom.* W *is the fully screened interaction. The definitions of the models are summarized in Table 1 below. The left and right figures correspond respectively to the real and imaginary parts of* U *[20].*

The on-site Hubbard U as a function of frequency for several choices of d-subspace is illustrated in Fig. 4. Several conclusions can be drawn from examining the imaginary part of W and U. $\mathrm{Im}(W)$ exhibits several sharp peaks, which correspond to collective excitations in the system. The peak at 2 eV arises from collective charge oscillations (plasmons) of electrons in the t_{2g}-bands whereas the peak at 15 eV corresponds to a plasmon excitation of electrons in the whole system. In the t_{2g}-model and other models, the peak at 2 eV disappears, which confirms the interpretation of it as a collective excitation of the t_{2g}-electrons since polarizations within the t_{2g}-bands are excluded in the models. We can also conclude that the 15 eV plasmon is dominated by the oxygen p-to-vanadium $3d$ transitions since this peak disappears in the dp-model in which p-to-d polarizations are excluded. The p-to-e_g polarizations are apparently stronger than the p-to-t_{2g} polarizations since in going from the t_{2g}-model to the $(t_{2g} + p)$-model, the plasmon peak at 15 eV is greatly reduced. As can be seen on the left of Fig. 4 the real part of U becomes increasingly constant as the d-subspace is enlarged and eventually it will approach the bare Coulomb interaction value, as expected.

Table 1: *Definitions of models*

model:	t_{2g}	d	t_{2g}+p	dp
d- subspace:	V t_{2g}	V ($t_{2g} + e_g$)	V t_{2g}+O p	V ($t_{2g} + e_g$)+O p

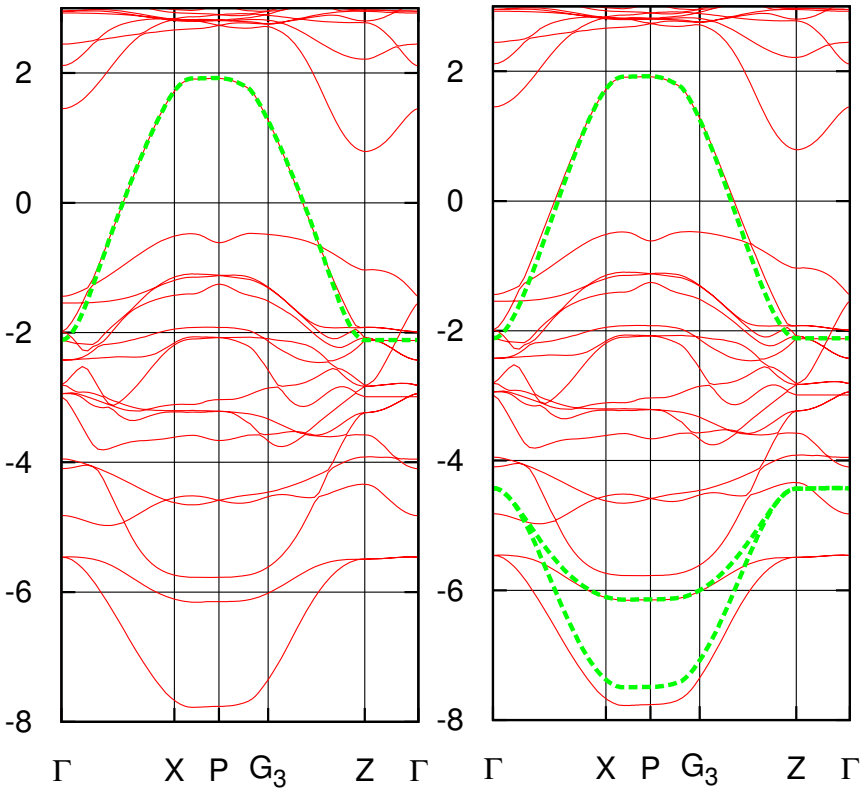

Fig. 5: *LDA band structure of La_2CuO_4. The green dashed lines are the bands obtained from the Wannier orbitals and represent the d-subspace. Left figure: one-band model (anti-bonding O $p_{x,y}$-Cu $d_{x^2-y^2}$). Right figure: Emery's three-band model (Cu $d_{x^2-y^2}$ and O p_x, p_y) [21].*

3.2 Undoped cuprate La_2CuO_4

The LDA band structure of La_2CuO_4, the parent compound of a prototype of high-temperature superconductors, is displayed in Fig. 5. The relevant bands arise from the copper $d_{x^2-y^2}$ orbital and the two oxygen p_x and p_y orbitals on the CuO_2 plane in which superconductivity is believed to originate. Since the bands to be modelled are not entirely isolated, the disentanglement procedure described in a previous section has been applied and the bands generated from the Wannier orbitals do not completely reproduce the original LDA bands.

The effective one-band model consists of a single orbital of $d_{x^2-y^2}$ character at each Cu site. The three-band model includes also the two in-plane Wannier orbitals of O p_x/p_y character. Although the conduction bands in the two models look very similar the Wannier orbitals corresponding to the Cu $d_{x^2-y^2}$ character are actually very different. In the one-band model the Cu-centered Wannier orbital is constructed from a few bands close to the Fermi energy, which leads to more delocalized Wannier orbitals than in the three-band model, in which more states are used to construct the Wannier orbitals. In the one-band model there is a one-to-one correspondence between the conduction band and the Wannier orbital of $d_{x^2-y^2}$-character spanning the d-subspace, while in the three-band model the conduction band is the antibonding combination of the p- and d-states and the two valence bands are the bonding and nonbonding combinations. The main d-weight is in the conduction band but there is also a small d-weight in the valence bands.

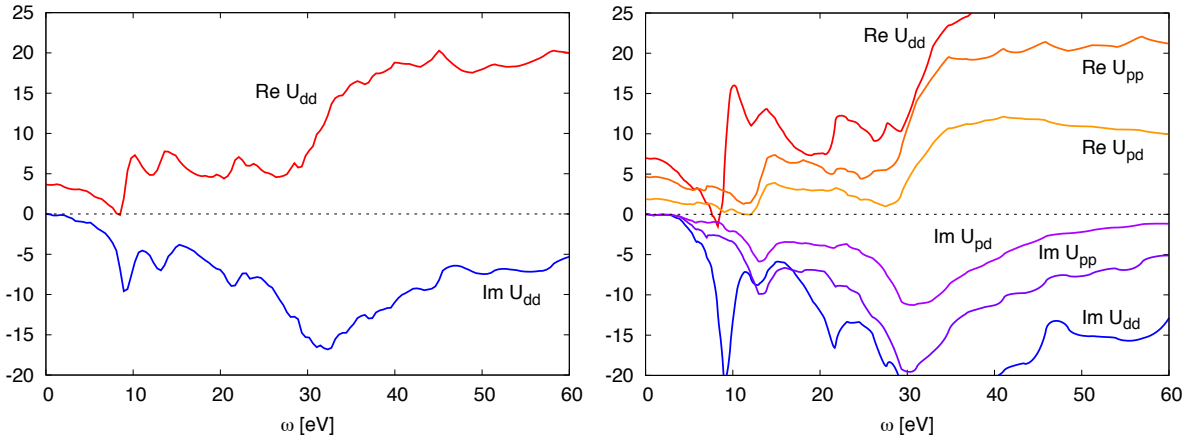

Fig. 6: *The Hubbard U for La_2CuO_4 for the one-band model (left panel) and the three-band model (right panel). U_{dd} and U_{pp} are respectively the on-site U on the copper and oxygen sites and U_{pd} is the off-site U between the copper and oxygen sites [21].*

The Hubbard U for the one- and three-band models are shown in Fig. 6. It is to be noted that in both models, only transitions within the conduction band are excluded when calculating U. From the point of view of cRPA, the d-subspace is spanned by the conduction band only. The strong peak at 9 eV can be traced back to p-to-d transitions corresponding to the collective charge oscillation of the oxygen p-electrons. It is interesting to note that the peak is not present in U_{pp}, indicating that the collective excitation has its main weight on the copper site [21]. A comparison between the left and right panels of Fig. 6 suggests different magnitudes of U for the two models. The reason for the larger magnitude of U_{dd} in the three-band model is due mainly to the more localized Wannier orbital. In the full three-band model in which the oxygen p-orbitals are treated as part of the d-subspace, the magnitude of U will be even larger since p-to-d transitions are excluded when computing U.
Noteworthy is the significant size of the off-site U_{pd}, which evidently should not be neglected. It may, however, be sufficient to treat the effects of U_{pd} at the mean-field level.

3.3 Early lanthanides series

As a further example, the static U corresponding to the $4f$-bands of the early lanthanides series is shown in Fig. 7 (left) together with experimental estimates from XPS and BIS spectra. The cRPA values tend to be lower than the experimental estimates but noticeably follow the trend across the series rather closely and especially the jump at Eu and Gd is correctly captured [22]. The lower cRPA values are most likely due to the well known LDA problem in describing the band structure of the $4f$-series. Gadolinium may serve as an illustration for the problem with the LDA. In Fig. 8 the LDA $4f$ density of states is compared with that of the LDA+U, the latter is known to be in good agreement with the experimental photoemission and inverse photoemission data. As can be seen, the LDA exchange splitting separating the occupied and unoccupied $4f$-bands is severely underestimated. Since the LDA $4f$-bands are too close to the Fermi level, cRPA calculations based on this LDA band structure overestimate screening and result in too small U. Indeed, when the band structure is calculated self-consistently within

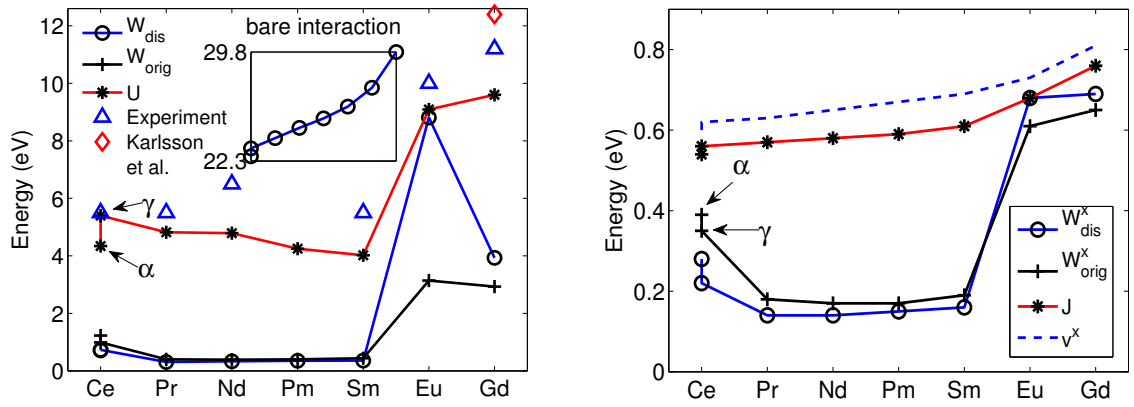

Fig. 7: *Left: The average diagonal matrix element of the fully screened interaction W and the Hubbard U for the lanthanides at $\omega = 0$. W is calculated both using the original states (W_{orig}) and the disentangled states (W_{dis}). The experimental data are estimations of U from XPS and BIS spectra. The inset shows the average diagonal element of the bare interaction across the series. Right: The average exchange matrix element of the fully screened interaction (W^x), the partially screened interaction (J) and the bare interaction (v^x) for the lanthanides [22].*

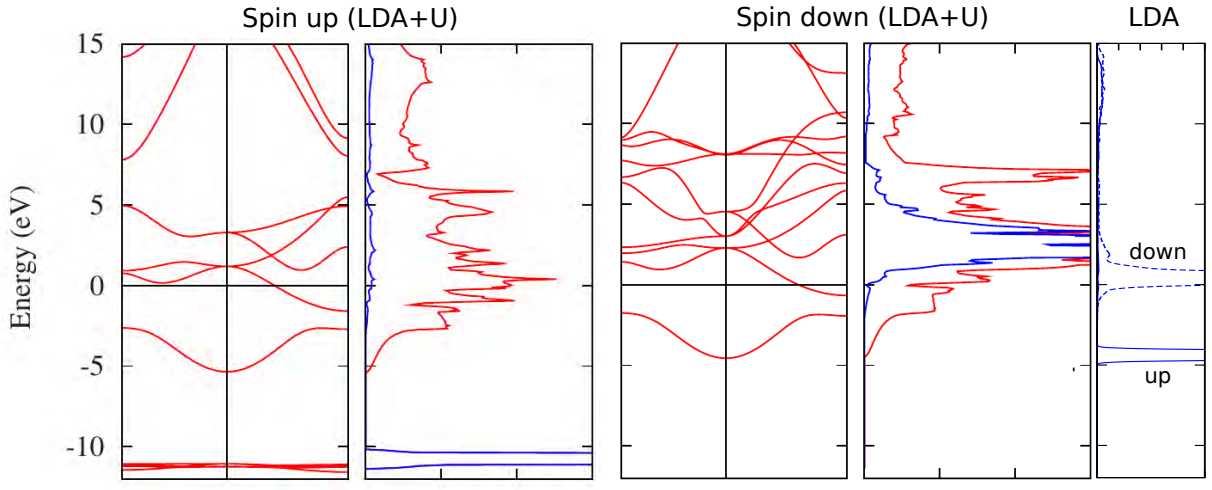

Fig. 8: *LDA+U band structure, density of states (DOS) and partial f-DOS (blue) for gadolinium. The calculations were done using the parameters U = 12.4 eV and J = 1.0 eV. The experimental exchange splitting is approximately 12-13 eV. The displayed directions are $\frac{1}{2}(1,1,1) \rightarrow \Gamma \rightarrow (1,0,0)$. For comparison, we also show the partial f-DOS from a spin-polarized LDA calculation [23].*

the LDA+U scheme, the cRPA value increases significantly and in better agreement with the experimental estimate [24]. This illustrates the importance of the one-particle part of the model Hamiltonian in capturing the correct Coulomb correlations.

In Fig. 7 (right) the exchange J across the series is also shown and compared with the bare values. It can be seen that the common procedure for approximating J by its unscreened atomic value is quite reasonable. This is as anticipated since the exchange interaction, which does not contain a $l = 0$ charge component, is relatively immune to screening.

Since the $4f$-bands are entangled, as can be seen, e.g., in the case of gadolinium, the disentanglement procedure described above is also applied here. To measure quantitatively the quality of the disentangled band structure, the fully screened interactions computed using the original and disentangled band structures are compared in Fig. 7. With the exception of Eu, the small difference between the two indicates that the entangled band structure provides a good representation of the original band structure.

4 Summary

The reliable determination of the Hubbard U based on a realistic band structure of a given material has become feasible, allowing for a first-principles study of the electronic structure of strongly correlated materials. Theoretical calculations of the Hubbard U eliminate uncertainties and ambiguities associated with treating U as adjustable parameters. By analyzing the effects of the individual screening channels on the screened interaction, we can discern which screening channels are important, providing valuable physical insights and a guide for constructing a model Hamiltonian.

Acknowledgments

Financial support from the Swedish Research Council (VR) is gratefully acknowledged.

Appendix

A Response functions from Green function formalism

The response functions can be derived from Green function by introducing a probing time-dependent field $\varphi(\mathbf{r},t)$ that couples to the charge density. In the presence of a time-dependent field it is convenient to work in the Dirac or interaction representation. In this representation the Green function is defined as, with the notation $1=(\mathbf{r}_1,t_1)$ etc.,

$$iG(1,2)=\frac{\langle\Psi_0|T[\hat{S}\hat{\psi}_D(1)\hat{\psi}_D(2)]|\Psi_0\rangle}{\langle\Psi_0|\hat{S}|\Psi_0\rangle} \tag{61}$$

where Ψ_0 is the many-electron ground state, $\hat{\psi}_D$ is the field operator in the interaction picture

$$\hat{\psi}_D(\mathbf{r},t)=e^{i\hat{H}t}\hat{\psi}(\mathbf{r})e^{-i\hat{H}t}, \tag{62}$$

where $\hat{H}$ is the many-electron Hamiltonian without the probing field $\varphi(\mathbf{r},t)$. It is worth noting that in the interaction picture, the field operator does not depend on the probing field φ. The time-ordering operator T chronologically orders the field operators so that the operator containing the earliest time stands farthest to the right. $\hat{S}$ is the scattering operator

$$\hat{S}=\hat{U}_D(\infty,-\infty), \tag{63}$$

where $\hat{U}_D$ is the time-evolution operator in the interaction picture

$$\hat{U}_D(t,t')=T\exp\left(-i\int_{t'}^{t}d\tau\,\hat{\phi}(\tau)\right), \tag{64}$$

and

$$\hat{\phi}(t)=\int d^3r\,\hat{\rho}(\mathbf{r},t)\,\varphi(\mathbf{r},t). \tag{65}$$

The Green function satisfies the equation of motion

$$\left(i\frac{\partial}{\partial t_1}-h(1)\right)G(1,2)-\int d3\,\Sigma(1,3)\,G(3,2)=\delta(1-2), \tag{66}$$

where h is the one-particle part of the Hamiltonian that includes the probing field φ and the Hartree potential V_{H}

$$h=-\frac{1}{2}\nabla^2+V_{\mathrm{ext}}+V_{\mathrm{H}}+\varphi. \tag{67}$$

The time-ordered linear density response function is defined as

$$R(1,2)=\frac{\delta\rho(1)}{\delta\varphi(2)}. \tag{68}$$

It is advantageous to work with the time-ordered response function since we are not restricted to $t_1>t_2$, as in the case of the retarded version, so the functional derivative can be taken freely. The charge density can be obtained from the diagonal element of the Green function

$$\rho(1)=-iG(1,1^+), \tag{69}$$

where 1^+ indicates that $t_1^+ = t_1 + \eta$ where η is a positive infinitesimal. When taking the functional derivative of G with respect to the probing field φ, only the scattering operator $\hat{S}$ is affected since the field operator in the interaction picture is independent of φ. The functional derivative of $\hat{S}$ with respect to φ is given by

$$\frac{\delta \hat{S}}{\delta\varphi(2)} = \frac{\delta}{\delta\varphi(2)} T \exp\left(-i\int d1\, \hat{\rho}(1)\,\varphi(1)\right) = -iT\left(\hat{S}\,\hat{\rho}(2)\right). \tag{70}$$

The response function is then

$$\begin{aligned} R(1,2) = \frac{\delta\rho(1)}{\delta\varphi(2)} &= -i\,\frac{\delta G(1,1^+)}{\delta\varphi(2)} = \frac{\delta}{\delta\varphi(2)} \frac{\left\langle \Psi \left| T\left(\hat{S}\hat{\rho}_D(1)\right)\right| \Psi\right\rangle}{\left\langle \Psi \left| \hat{S} \right| \Psi\right\rangle} \\ &= -\frac{i\left\langle \Psi \left| T\left(\hat{S}\hat{\rho}_D(2)\hat{\rho}_D(1)\right)\right| \Psi\right\rangle}{\left\langle \Psi \left| \hat{S} \right| \Psi\right\rangle} + \frac{i\left\langle \Psi \left| T\left(\hat{S}\hat{\rho}_D(1)\right)\right| \Psi\right\rangle \left\langle \Psi \left| T\left(\hat{S}\hat{\rho}_D(2)\right)\right| \Psi\right\rangle}{\left\langle \Psi \left| \hat{S} \right| \Psi\right\rangle^2} \end{aligned} \tag{71}$$

After taking the functional derivative of the density $\rho(1) = -iG(1,1^{+)}$ with respect to the applied field φ, we set $\varphi = 0$. This implies that $\hat{S} = 1$ and the Dirac field operator becomes the Heisenberg field operator. We obtain the time-ordered linear density response function

$$iR(1,2) = \langle\Psi|\Delta\hat{\rho}_H(2)\Delta\hat{\rho}_H(1)|\Psi\rangle\,\theta(t_2 - t_1) + \langle\Psi|\Delta\hat{\rho}_H(1)\Delta\hat{\rho}_H(2)|\Psi\rangle\,\theta(t_1 - t_2)\,, \tag{72}$$

where the density fluctuation operator is given by

$$\Delta\hat{\rho}_H(1) = \hat{\rho}_H(1) - \rho(1)\,. \tag{73}$$

To obtain the response function in the frequency representation we first insert a complete set of eigenstates of $\hat{H}$ in between the density operators and use the definition of the Heisenberg operator, yielding

$$\begin{aligned} iR(1,2) &= \sum_n \left\langle \Psi_0 \left| e^{i\hat{H}t_2}\Delta\hat{\rho}(\mathbf{r}_2)e^{-i\hat{H}t_2}\right| \Psi_n\right\rangle \left\langle \Psi_n \left| e^{i\hat{H}t_1}\Delta\hat{\rho}(\mathbf{r}_1)e^{-i\hat{H}t_1}\right| \Psi\right\rangle \theta(t_2 - t_1) \\ &+ \sum_n \left\langle \Psi_0 \left| e^{i\hat{H}t_1}\Delta\hat{\rho}(\mathbf{r}_1)e^{-i\hat{H}t_1}\right| \Psi_n\right\rangle \left\langle \Psi_n \left| e^{i\hat{H}t_2}\Delta\hat{\rho}(\mathbf{r}_2)e^{-i\hat{H}t_2}\right| \Psi_0\right\rangle \theta(t_1 - t_2) \\ &= \sum_n \langle\Psi_0|\Delta\hat{\rho}(\mathbf{r}_2)\,|\Psi_n\rangle\,\langle\Psi_n|\,\Delta\hat{\rho}(\mathbf{r}_1)|\Psi_0\rangle\, e^{-i(E_n - E_0)(t_2 - t_1)}\theta(t_2 - t_1) \\ &+ \sum_n \langle\Psi_0|\Delta\hat{\rho}(\mathbf{r}_1)\,|\Psi_n\rangle\,\langle\Psi_n|\,\Delta\hat{\rho}(\mathbf{r}_2)|\Psi_0\rangle\, e^{-i(E_n - E_0)(t_1 - t_2)}\theta(t_1 - t_2) \end{aligned} \tag{74}$$

Performing the Fourier transform $\int d\tau\, \exp(i\omega\tau)R(\tau)$, where $\tau = t_1 - t_2$, yields

$$R(\mathbf{r},\mathbf{r}';\omega) = \sum_n \left[\frac{\langle\Psi_0|\Delta\hat{\rho}(\mathbf{r})\,|\Psi_n\rangle\,\langle\Psi_n|\,\Delta\hat{\rho}(\mathbf{r}')|\Psi_0\rangle}{\omega - E_n + E_0 + i\eta} - \frac{\langle\Psi_0|\Delta\hat{\rho}(\mathbf{r}')\,|\Psi_n\rangle\,\langle\Psi_n|\,\Delta\hat{\rho}(\mathbf{r})|\Psi_0\rangle}{\omega + E_n - E_0 - i\eta}\right]. \tag{75}$$

The corresponding retarded response function, the well-known Kubo's formula, is given by

$$R^{\rm ret}(\mathbf{r},\mathbf{r}';\omega) = \sum_n \left[\frac{\langle\Psi_0|\Delta\hat{\rho}(\mathbf{r})\,|\Psi_n\rangle\,\langle\Psi_n|\,\Delta\hat{\rho}(\mathbf{r}')|\Psi_0\rangle}{\omega - E_n + E_0 + i\eta} - \frac{\langle\Psi_0|\Delta\hat{\rho}(\mathbf{r}')\,|\Psi_n\rangle\,\langle\Psi_n|\,\Delta\hat{\rho}(\mathbf{r})|\Psi_0\rangle}{\omega + E_n - E_0 + i\eta} \right], \tag{76}$$

which, in contrast to the time-ordered one, has all poles in the lower half plane. The response function gives information about the excitation spectrum of the system: $\mathrm{Im}\,R(\omega)$ has peaks whenever $\omega = E_n - E_0$, corresponding to the N-particle excitation energies.
If there is no magnetic field, i.e., if time-reversal symmetry is obeyed,

$$\langle\Psi_0|\Delta\hat{\rho}(r')\,|\Psi_n\rangle\,\langle\Psi_n|\,\Delta\hat{\rho}(r)|\Psi_0\rangle = \langle\Psi_0|\Delta\hat{\rho}(r)\,|\Psi_n\rangle\,\langle\Psi_n|\,\Delta\hat{\rho}(r')|\Psi_0\rangle \tag{77}$$

is real so that R satisfies

$$R(\mathbf{r},\mathbf{r}';-\omega) = R(\mathbf{r},\mathbf{r}';\omega), \tag{78}$$

$$R(\mathbf{r},\mathbf{r}';\omega) = R(\mathbf{r}',\mathbf{r};\omega). \tag{79}$$

The response function R is the *time-ordered* response which differs from the *retarded* response $R^{\rm ret}$. The two are related as

$$\mathrm{Re}\,R(\omega) = \mathrm{Re}\,R^{\rm ret}(\omega), \tag{80}$$

$$\mathrm{Im}\,R(\omega)\mathrm{sgn}(\omega) = \mathrm{Im}\,R^{\rm ret}(\omega),\ \mathrm{sgn}(\omega) \equiv \omega/|\omega|, \tag{81}$$

valid for real ω.
Compared with the original derivation of Kubo, the Schwinger functional derivative technique provides a simple way of deriving the response functions. We have derived the Kubo formula specifically for linear density response function. However, the method is applicable to a more general response function since any expectation value of a single-particle operator in the ground state is expressible in terms of the Green function. Moreover, higher-order density response functions can be readily worked out. For example, calculating the second-order density response function given by

$$R(1,2,3) = \frac{\delta^2\rho(1)}{\delta\varphi(3)\,\delta\varphi(2)} = \frac{\delta R(1,2)}{\delta\varphi(3)}\,, \tag{82}$$

is just a matter of inserting $\delta\hat{S}/\delta\varphi$ at the appropriate places.
In reality, we must resort to approximations for the response function. A commonly used approximation is the RPA which can be derived from the equation of motion of the Green function in Eq. (66). We obtain after multiplying both sides of the equation by G^{-1}

$$\left(i\frac{\partial}{\partial t_1} - h(1)\right)\delta(1-2) - \Sigma(1,2) = G^{-1}(1,2), \tag{83}$$

Since

$$h = -\frac{1}{2}\nabla^2 + V_{\rm ext} + V_{\rm H} + \varphi \tag{84}$$

we find

$$\frac{\delta G^{-1}(1,2)}{\delta\varphi(3)} = -\delta(1-2)\left(\delta(1-3)+\frac{\delta V_{\rm H}(1)}{\delta\varphi(3)}\right) - \frac{\delta\Sigma(1,2)}{\delta\varphi(3)}\,. \tag{85}$$

We wish, however, to calculate $\delta G/\delta\varphi$, which can be obtained by using the identity

$$\int d4\left(\frac{\delta G^{-1}(1,4)}{\delta\varphi(3)}\,G(4,2) + G^{-1}(1,4)\,\frac{\delta G(4,2}{\delta\varphi(3)}\right) = 0\,, \tag{86}$$

which follows from taking the functional derivative with respect to φ of

$$\int d4\, G^{-1}(1,4)\, G(4,2) = \delta(1-2). \tag{87}$$

From Eq. (86) we find

$$\frac{\delta G(1,2)}{\delta\varphi(3)} = -\int d4\, d5\, G(1,4)\,\frac{\delta G^{-1}(4,5)}{\delta\varphi(3)}\,G(5,2). \tag{88}$$

The response function is then

$$R(1,2) = \frac{\delta\rho(1)}{\delta\varphi(2)} = -i\,\frac{\delta G(1,1^+)}{\delta\varphi(2)} = i\int d3\, d4\, G(1,3)\,\frac{\delta G^{-1}(3,4)}{\delta\varphi(2)}\,G(4,1^+). \tag{89}$$

Using Eq. (85) with $\delta\Sigma/\delta\varphi = 0$ yields the RPA

$$\begin{aligned} R(1,2) &= -i\int d3\, d4\, G(1,3)\,\delta(3-4)\left(\delta(3-2)+\frac{\delta V_{\rm H}(3)}{\delta\varphi(2)}\right)G(4,1^+) \\ &= -i\int d3\, G(1,3)\left(\delta(3-2)+\frac{\delta V_{\rm H}(3)}{\delta\varphi(2)}\right)G(3,1^+). \end{aligned} \tag{90}$$

Identifying the polarization function as

$$P(1,2) = -iG(1,2)\,G(2,1^+) \tag{91}$$

and using

$$V_{\rm H}(3) = \int d4\, v(3-4)\,\rho(4) \tag{92}$$

we obtain the RPA equation

$$R(1,2) = P(1,2) + \int d3\, d4\, P(1,3)\, v(3-4)\, R(4,2)\,. \tag{93}$$

Using the convolution theorem, the Fourier transform of the polarization function becomes

$$P(\mathbf{r},\mathbf{r}';\omega) = -i\int\frac{d\omega'}{2\pi}G(\mathbf{r},\mathbf{r}';\omega+\omega')\,G(\mathbf{r}',\mathbf{r};\omega'). \tag{94}$$

If we use a non-interacting Green function,

$$G^0(\mathbf{r},\mathbf{r}';\omega) = \sum_n^{\rm occ}\frac{\psi_n(\mathbf{r})\psi_n^*(\mathbf{r}')}{\omega-\varepsilon_n-i\delta} + \sum_n^{\rm unocc}\frac{\psi_n(\mathbf{r})\psi_n^*(\mathbf{r}')}{\omega-\varepsilon_n+i\delta}, \tag{95}$$

and perform the frequency integral, we obtain the expression in Eq. (34). The RPA is sometimes referred to as the time-dependent Hartree approximation because when calculating the response function only the change in the Hartree potential with respect to the probing field is taken into account whereas the change in the self-energy, $\delta\Sigma/\delta\varphi$, is neglected.

References

[1] J. Hubbard, Proc. Royal Soc. London A **276**, 238 (1963)

[2] H. Jones, Rev. Mod. Phys. **87**, 897 (2015)

[3] A. Georges, G. Kotliar, W. Krauth, and M.J. Rozenberg, Rev. Mod. Phys. **68**, 13 (1996)

[4] C. Herring: *Exchange interactions among itinerant electrons*, Vol. 4 of G.T. Rado and H. Suhl (eds.): *Magnetism* (Academic Press, New York, 1966)

[5] B.N. Cox, M.A. Coultard, and P. Loyd, J. Phys. F.: Metal Physics **4**, 807 (1974)

[6] J.F. Herbst, R.E. Watson, and J.W. Wilkins, Phys. Rev. B **17**, 3089 (1978)

[7] P.H. Dederichs, S. Blügel, R. Zeller, and H. Akai, Phys. Rev. Lett. **53**, 2512 (1984)

[8] O. Gunnarsson, O.K. Andersen, O. Jepsen, and J. Zaanen, Phys. Rev. B **39**, 1708 (1989)

[9] M.S. Hybertsen, M. Schlüter, N.E. Christensen, Phys. Rev. B **39**, 9028 (1989)

[10] M. Cococcioni and S. de Gironcoli, Phys. Rev. B **71**, 035105 (2005)

[11] F. Aryasetiawan, M. Imada, A. Georges, G. Kotliar, S. Biermann, and A.I. Lichtenstein, Phys. Rev. B **70**, 195104 (2004)

[12] L. Hedin, Phys. Rev. **139**, A796 (1965)

[13] L. Hedin and S. Lundqvist in Vol. 23, H. Ehrenreich, F. Seitz, and D. Turnbull (eds.): *Solid State Physics* (Academic, New York, 1969)

[14] F. Aryasetiawan and O. Gunnarsson, Rep. Prog. Phys. **61**, 237 (1998)

[15] A.L. Fetter and J.D. Walecka: *Quantum Theory of Many-Particle Systems* (McGraw-Hill, New York, 1971)

[16] D. Pines: *Elementary Excitations in Solids* (Benjamin, New York, 1963)

[17] O.K. Andersen, Phys. Rev. B **12**, 3060 (1975)

[18] N. Marzari and D. Vanderbilt, Phys. Rev. B **56**, 12847 (1997)

[19] T. Miyake, F. Aryasetiawan, and M. Imada, Phys. Rev. B **80**, 155134 (2009)

[20] Chapter 7 of E. Pavarini, E. Koch, D. Vollhardt, and A.I. Lichtenstein (eds.): *The LDA+DMFT Approach to Strongly Correlated Materials*, Reihe Modeling and Simulation, Vol. 1 (Forschungszentrum Jülich, 2011) `http://www.cond-mat.de/events/correl11`

[21] P. Werner, R. Sakuma, F. Nilsson, and F. Aryasetiawan, Phys. Rev. B **91**, 125142 (2015)

[22] F. Nilsson, R. Sakuma, and F. Aryasetiawan, Phys. Rev. B **88**, 125123 (2013)

[23] F. Nilsson and F. Aryasetiawan, Computation **6**, 26 (2018)

[24] K. Karlsson, F. Aryasetiawan, and O. Jepsen, Phys. Rev. B **81**, 245113 (2010)